論 文 の 内 容 の 要 旨

論文題目　**Inclusive modeling of hydrate formation in sand sediment for sub-seabed CO_2 storage**（海底下二酸化炭素貯留のための砂層内ハイドレート生成に関する包括的モデル構築の研究）

氏　　名　于 涛

1. Introduction

Global warming has been one of the most serious issues for decades mainly due to CO_2 emission into the atmosphere, and CO_2 capture and storage (CCS) is expected to be one of the most effective strategies against it.

For CO_2 storage in the deep saline aquifers in the ocean, there is a social concern that it may have inadequate safe storage life span because the stored CO_2 may not remain stable beneath the seafloor. As a novel approach, CO_2 storage in the deep saline aquifers using the sealing effect of gas hydrate (hydrate sealing) was proposed by Koide et al. [1]. In this method, if a leakage occurs at the sub-seabed storage sites, and CO_2 gas seeps out of the cap rock which is considered to be the first seal, the leaked CO_2 gas migrates upward and tends to form CO_2 hydrate at the base of the hydrate stability zone, creating a low-permeability secondary cap layer which can greatly restrict further upward CO_2 flow.

On the other hand, as a new countermeasure, CO_2 storage in the sub-seabed sand sediment in the form of gas hydrate (hydrate storage) was proposed by Inui et al. [2]. In this method, CO_2 gas is injected into the sub-seabed sediment at the depth of about hundreds of meters beneath the seafloor under the water column of more than 300 m, where the sediment is composed by alternate sand-mud layers under the condition of low temperature and high pressure. After injection, CO_2 gas selectively flows into the sand layers whose permeability is 10~100 times higher than the surrounding mud layers, and forms CO_2 hydrate gradually. As a result, CO_2 can be stored safely in the sand sediment in the form of gas hydrate.

In order to evaluate the potential and feasibility of these two methods precisely, an inclusive model for CO_2 hydrate formation, which includes different hydrate formation morphologies at different locations in the sand sediment, is proposed in this study. Then, numerical simulations are conducted using this new inclusive model to determine the unknown model parameters. In addition, the inclusive model is validated by the experimental results of CO_2 hydrate formation in the lab-scale sediment by liquid CO_2 injection.

2. Inclusive modeling of CO_2 hydrate formation in lab-scale sand sediment

2.1 Inclusive model for CO_2 hydrate formation in the sand sediment

In this study, an inclusive model for CO_2 hydrate formation in the sand sediment is proposed as below:

$$Q_H = \delta Q_{H1} + Q_{H2} + Q_{H3}. \tag{1}$$

As shown in Fig. 1, in this model, hydrate formation morphologies in the sand sediment are assumed to consist of three different parts: (a) on the gas front, (b) on the hydrate film behind the gas front, and (c) on the surface of the sand particles behind the gas front, where the corresponding CO_2 hydrate formation rates are Q_{H1}, Q_{H2}, and Q_{H3}, respectively.

δ in the model is a "switch", which is used to decide whether the gas front exists in a computational cell or not. It is defined as below:

$$\delta = \begin{cases} 1 & \cdots \text{ in a cell where the gas front exists} \\ 0 & \cdots \text{ elsewhere} \end{cases}. \tag{2}$$

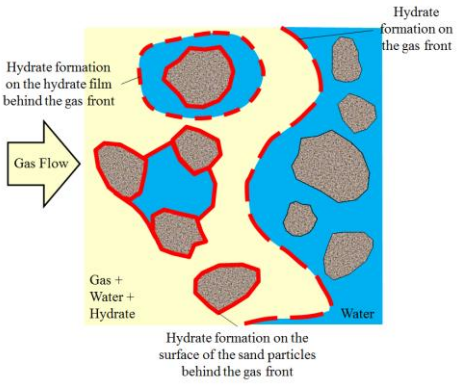

Fig. 1 The schematic diagram of hydrate formation morphologies in the sand sediment proposed in this study

2.1.1 Hydrate formation rate on the gas front

Hydrate formation rate on the gas front is considered to be composed of the fresh surface formation (rupture), the growth of the hydrate film, and the formation loss due to the capture of the sand particles, which is given as below:

$$Q_{H1} = k_f x_1 A_1 \left(f_G^{CO_2} - f_{eq}^{CO_2} \right) + k_f \left(1 - x_1\right) A_1 \left(f_{I1}^{CO_2} - f_{eq}^{CO_2} \right) - Q_{H1\to 3}, \tag{3}$$

where k_f is the intrinsic rate constant of CO_2 hydrate formation [mol/m^2/Pa/s], A_1 is the gas-liquid interfacial area [m^2/m^3], and x_1 is the rupture ratio on the gas front [-]. Besides, $f_G^{CO_2}$, $f_{I1}^{CO_2}$, and $f_{eq}^{CO_2}$ are CO_2 fugacity in the gas phase, at the gas-liquid interface on the gas front, and at the three-phase equilibrium point [Pa], respectively.

The rupture ratio on the gas front x_1 is defined as below:

$$x_1 = \alpha \frac{(1-\phi)}{\phi} \cdot \frac{|U_G|}{r}, \tag{4}$$

where α is the function of geometrical factor and microscale induction time [s]. ϕ is the porosity of the sand sediment [-], U_G is the velocity of the gas flow [m/s], and r is the radius of the sand particles [m].

$Q_{H1\to3}$ is the negative formation rate transferred from the part of hydrate captured by the sand particles, which is calculated as below:

$$Q_{H1\to3} = \frac{\rho_H}{M_H} \cdot \frac{(1-\phi)}{\phi^2} \cdot \frac{h_1}{r} \cdot A_1 \cdot |U_G|, \tag{5}$$

where ρ_H and M_H are the density [kg/m^3] and molar mass [kg/mol] of CO_2 hydrate, respectively. h_1 is the average thickness of the hydrate film on the gas front [m].

2.1.2 Hydrate formation rate on the hydrate film behind the gas front

Hydrate forms on the hydrate film behind the gas front at two different locations: one is at the fresh surface (rupture), and the other one is at the gas-liquid interface of the existing hydrate film (the growth of the hydrate film). The corresponding hydrate formation rate is given as below:

$$Q_{H2} = k_f x_2 A_2 \left(f_G^{CO_2} - f_{eq}^{CO_2} \right) + k_f (1-x_2) A_2 \left(f_{I2}^{CO_2} - f_{eq}^{CO_2} \right), \tag{6}$$

where A_2 is the gas-liquid interfacial area behind the gas front [m^2/m^3], x_2 is the rupture ratio behind the gas front, and $f_{I2}^{CO_2}$ is CO_2 fugacity at the gas-liquid interface behind the gas front [Pa].

The rupture ratio model proposed by Takahashi et al. [3] is adopted in this study as below:

$$x_2 = \exp\left(-\beta h_2^2\right), \tag{7}$$

where β is an unknown model coefficient [m^{-2}], and h_2 is the average thickness of the hydrate film behind the gas front [m].

2.1.3 Hydrate formation rate on the surface of the sand particles behind the gas front

Hydrate forms on the surface of the sand particles behind the gas front from two different parts: one is dissolved CO_2 in the aqueous phase, and the other one is the part of hydrate captured by the sand particles as mentioned before. Therefore, Q_{H3} is given as below:

$$Q_{H3} = k_f A_S \left(f_A^{CO_2} - f_{eq}^{CO_2} \right) + \delta Q_{H1\to3}, \tag{8}$$

where A_S is the sand surface area [m^2/m^3], and $f_A^{CO_2}$ is CO_2 fugacity in the aqueous phase [Pa].

2.2 Modified permeability reduction model

Since hydrate formation morphologies are classified by locations in this study, it is considered that CO_2 hydrate formation with different morphologies should have different contributions to the permeability reduction. Therefore, a modified permeability reduction model is proposed as below:

$$k_S = k_{S,0} K_{H1} K_{H2} K_{H3}, \tag{9}$$

where k_S and $k_{S,0}$ are the permeability of the sand sediment with and without hydrate [m^2]. K_{H1}, K_{H2}, and K_{H3} are the permeability reduction coefficients of hydrate formation on the gas front, on the hydrate film, and on the surface of the sand particles behind the gas front [-], respectively, which are given as below:

$$K_{H1} = 1, \tag{10}$$

$$K_{H2} = (1 - S_{H2})^N, \tag{11}$$

$$K_{H3} = (1 - S_{H3})^3 \left[\frac{1-\phi}{1-\phi(1-S_{H3})} \right]^{\frac{4}{3}}, \tag{12}$$

where S_{H2} and S_{H3} are CO_2 hydrate saturation on the hydrate film, and on the surface of the sand particles behind the gas front [-], respectively. N is the permeability reduction exponent of hydrate formation behind the gas front [-].

3. Determination of model parameters

3.1 CO_2 hydrate formation without gas-liquid two-phase flow

The experiments of CO_2 hydrate formation in the lab-scale sand sediment without gas-liquid two-phase flow were carried out by Inui [4]. Then, in order to determine the intrinsic rate constant of CO_2 hydrate formation k_f and CO_2 diffusion constant in the hydrate film k_d, simulations of CO_2 hydrate formation in the lab-scale sand sediment without gas-liquid two-phase flow are conducted under the experimental conditions for five cases (Case 1~Case 5). Moreover, the fitting results are plotted by Arrhenius equation. By Arrhenius plot, the pre-exponential factor k_0 as 1.73×10^{13} mol/m^2/Pa/s, and the activation energy ΔE as 115.6 kJ are determined for k_f. On the other hand, k_d is determined by the average value of 3.30×10^{-18} mol/m/Pa/s. Besides, β is determined by an order of 10^{13} m^{-2} ($1.0\sim8.0\times10^{13}$ m^{-2}) under non-flow condition.

3.2 CO_2 hydrate formation with gas-liquid two-phase flow

The experiments of CO_2 hydrate formation in the lab-scale sand sediment with gas-liquid two-phase flow were carried out by Inui [4]. Then, in order to determine the unknown parameters α in Equation (4), β in Equation (7) and N in Equation (11), simulations of CO_2 hydrate formation in the lab-scale sand sediment with gas-liquid two-phase flow are conducted under the experimental conditions for two cases (Case 6 and Case 7).

By parameter-fitting, α, β, and N are determined as 1 s, 5.0×10^{10} m^{-2}, and 15.5, respectively. Fig. 2 shows the comparisons between the calculation results and the experimental data for temperature, differential pressure, and the amount of discharged water in Case 6 and Case 7. During the induction stage, as the gas front moves down towards the outlet gradually, CO_2 gas dissolves into the aqueous phase through the gas-liquid interface. After the induction stage, hydrate forms on the gas front and in the water-unsaturated zone behind the gas front. The differential pressure rise due to the blockage of the gas flow is replicated in Case 6. Compared with the experimental data, the timings of the temperature rises detected at T3~T7 are delayed in Case 6, mainly because the flow resistance in the sand sediment is so large that the gas flow has been slowed. However, the temperature jumps due to hydrate formation are replicated and confirmed by calculations. Besides, the calculated amount of discharged water is a little less than the experimental data in both the two cases, because most of the water forms hydrate or remains in the sand sediment as irreducible water instead of being discharged.

4. Validation of the inclusive model for CO_2 hydrate formation

The experiments of CO_2 hydrate formation in the lab-scale sediment by liquid CO_2 injection were carried out by Li et al. [4]. Then, in order to validate the inclusive model for CO_2 hydrate formation proposed in this study, simulations of CO_2 hydrate formation in the lab-scale sediment by liquid CO_2 injection are conducted under the experimental conditions for two cases (Case 8 and Case 9). Fig. 3 shows the comparisons between the calculation results and the experimental data for temperature changes in Case 8. It can be seen that the calculation results of the temperature changes detected at TC.4, TC.5, TC.6, TC.8, and TC.10, which increase greatly in the whole calculation period, fail to match the experimental data due to the broader distribution of liquid CO_2 in the sediment in the calculation than that in the experiment. However, the temperature changes detected at TC.2, TC.3, TC.7, and TC. 9 in the experiments, which are all the thermocouples near the liquid CO_2 inlet, are replicated and confirmed by calculations successfully, which validates the inclusive model for CO_2 hydrate formation proposed in this study to some extent.

5. Conclusion

An inclusive model for CO_2 hydrate formation is proposed in this study in order to figure out CO_2 hydrate formation morphologies, which are classified by locations in the sand sediment: i.e. on the gas front, on the hydrate film, and on the surface of the sand particles behind the gas front. Then, the processes of gas-liquid two-phase flow and CO_2 hydrate formation in the sand sediment under the experimental conditions are analyzed using a numerical simulator which incorporates this newly proposed hydrate formation model. Simulation results are compared with the experimental data, so that unknown parameters in the models are determined by parameter-fitting.

Besides, the inclusive model for CO_2 hydrate formation has been validated by the experimental results of CO_2 hydrate formation in the lab-scale sediment by liquid CO_2 injection to some extent.

References

[1] Koide, H., Takahashi, M., Tsukamoto, H., 1995. Self-trapping mechanisms of carbon dioxide in the aquifer disposal. *Energy Convers. Mgmt.*, 36(6-9), 505-508.

[2] Inui, M., Sato, T., Komai, T., Kagemoto, H., 2011. Experiments and numerical simulations of hydrate formation in sand sediment simulating sub-seabed CO_2 storage in the form of gas hydrate. *Journal of MMIJ*, 127(4-5), 194-201 (in Japanese).

[3] Takahashi, T., Sato, T., Inui, M., Hirabayashi, S., Brumby, P.E., 2012. Modeling of CO_2-hydrate formation at the gas-water interface in sand sediment. *Chem. Eng. Technol.*, 35(10), 1751-1758.

[4] Inui, M., 2011. Feasibility study on CO_2 sub-seabed storage in the form of gas hydrate. *Doctoral Dissertation: the University of Tokyo* (in Japanese).

[5] Li, Y.R., Someya, S., Yu, T., 2015. CO_2 sequestration under an artificial impermeable layer with clathrate hydrate in sediments. *Proc. 9th International Symposium on Measurement Techniques for Multiphase Flow, Sapporo, Japan*.

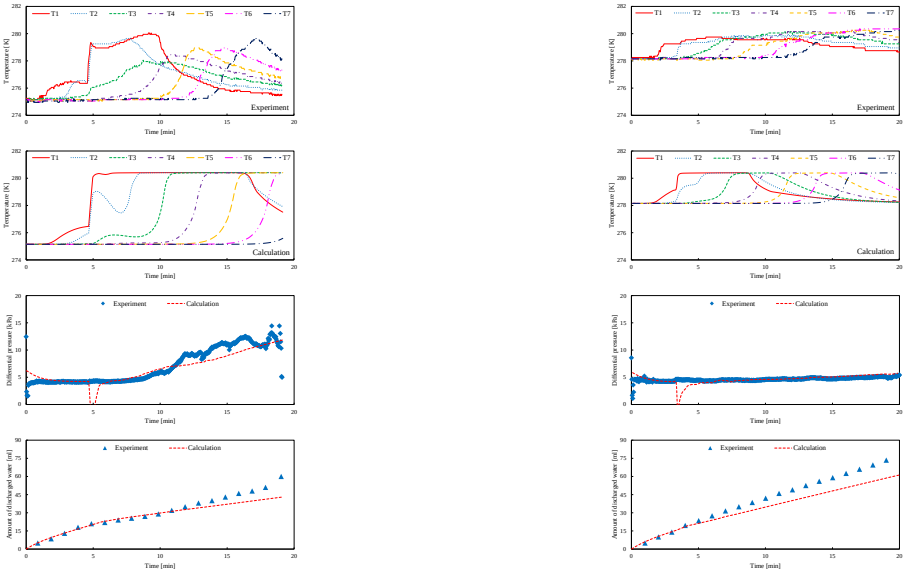

Fig. 2 The comparisons between the calculation results and the experimental data for temperature (first two ones), differential pressure (third ones), and the amount of discharged water (fourth ones) in Case 6 (275.15 K, 3.1 MPa) and Case 7 (278.15 K, 3.1 MPa)

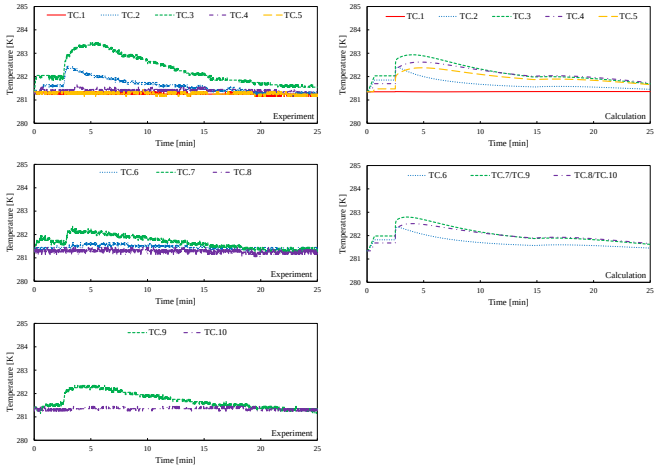

Fig. 3 The comparisons between the calculation results and the experimental data for temperature changes in Case 8 (281.35 K, 9.0 MPa)